ACTIVE CONTROL OF PASSIVE OCEAN ACOUSTIC FIELDS BY PROP-DRIVEN AUVS AND UNDERWATER GLIDERS

GL D'Spain Marine Physical Lab, Scripps Institution of Oceanography, USA
E Terrill Marine Physical Lab, Scripps Institution of Oceanography, USA
R Zimmerman Marine Physical Lab, Scripps Institution of Oceanography, USA
SA Jenkins Marine Physical Lab, Scripps Institution of Oceanography, USA
SD Lynch Marine Physical Lab, Scripps Institution of Oceanography, USA
JC Luby Applied Physics Lab, University of Washington, USA

1 INTRODUCTION

Synthetic aperture processing converts temporal processing gain into spatial gain through the use of a moving receiver and/or source. In active synthetic aperture, the source of the wave field energy used to image the environment is located on, and under control of, the platform creating the aperture. Aperture also can be synthesized without the use of an active source. In this passive case, the properties of the source are part of the set of unknowns to be determined and typically are the quantities of greatest interest.

The primary platform used to synthesize ocean acoustic aperture passively in this paper is an older-design, mid-size autonomous underwater vehicle (AUV). Mounted on its inner shroud is an 8-element hydrophone array with physical aperture in two horizontal dimensions, but overall size about a tenth of a wavelength at the low frequencies (200-500 Hz) of interest. Application of the concepts to the at-sea performance of a flying wing underwater glider also is presented. Hull-mounted acoustic arrays, versus towed arrays, retain an AUV's maneuverability and hydrodynamic efficiency. In addition, deployment/retrieval is much simpler, the relative positions of the array elements are independent of time, and the array data are not degraded during a maneuver. Although vehicle radiated acoustic and vibration noise is a more serious consideration, this self noise can be effectively eliminated in prop-driven AUVs[1] and is not present over most of the path of a buoyancy-driven glider. The major drawback of hull-mounted systems is that physical aperture is limited by vehicle size, thus motivating synthesis of aperture through motion.

The maneuverability and adaptability of an AUV equipped with a hull-mounted sonar system actually allows the vehicle to adapt its motion to purposefully impart a specific structure to the received field to optimize extraction of quantities of interest. This concept of active control of received acoustic fields through receiver motion is illustrated in this paper. An important consideration is the cost of motion due to the expenditure of energy available on the AUV.

2 SYNTHETIC APERTURE BEAMFORMING APPROACHES

2.1 Passive Synthetic Aperture Processing through Doppler Beamforming

Under plane wave propagation, synthetic aperture beamforming and Doppler processing are equivalent processes. For a single tone plane wave from a fixed source, the complex pressure recorded by a receiver moving at constant velocity v_r is

$$p_r(\omega_r, \vec{v}_r t) = A_p(\omega_s)\exp[i(\omega_s t + \vec{k}_s \bullet \vec{v}_r t)] = A_p(\omega_s)\exp[i\omega_r t] \quad (1)$$

The subscript "s" for the circular frequency, ω_s, and spatial frequency, $\vec{k}_s$ signifies that these quantities are those measured by a stationary receiver whereas the subscript "r" indicates a quantity measured by a moving receiver. The expression for the received frequency

$$\omega_r = \omega_s(1+\frac{v_r}{c_p}\cos[\theta_s - \psi_r]) \quad (2)$$

is the dispersion relation for sound propagating at phase velocity c_p to a moving receiver in a stationary medium[2]. The source azimuth is θ_s, the direction of receiver motion is ψ_r, and v_r without the over-arrow is the receiver speed. These equations show that all available information from synthetic aperture processing, including the sound field directionality, can be obtained by temporal processing through the frequency shifts due to motion of the receiver and the resulting redistribution of energy in the received pressure spectrum. Eqs. 1 and 2 also illustrate how passive synthetic aperture processing blurs the distinction between temporal and spatial frequency; the distribution of energy in the temporal frequency domain and the directional distribution of the acoustic sources become interdependent. This observation implies that to achieve significant array gains through creation of synthetic aperture in anisotropic ("acoustically cluttered") noise conditions, spectrally non-white noise conditions must also exist.

The Doppler beamforming process involves the integration of spectral energy collected over a set of straight-line tracks. The first step for a given assumed source frequency and assumed source azimuth (i.e., look direction) is to select a set of frequency bins, one from each straight-line track ("leg"). These frequency bins are determined by a cosine-dependent curve over leg number that is a function of source frequency and azimuth (Eq. 2). The average AUV speed and direction of motion for each leg, and the effective phase velocity of the received acoustic field, are taken as known inputs to the beamformer. In the case of moving physical aperture, the spectral levels are those measured by the physical beam pointed in the look direction of interest. The physical beams can be formed using conventional or adaptive beamforming techniques. The beamformer output then is the incoherent sum of the weighted spectral levels in these frequency bins.

A stationary source approximation can be made to reduce the number of source unknowns in the problem by abandoning any attempt to solve for information on the track of the moving source. Application of this assumption (a good approximation in most situations) results in two unknowns, the "effective" source frequency measured by a stationary receiver, ω_s, and source azimuth, θ_s.

The ambiguity surface (beamforming output) with Doppler/synthetic aperture processing for the simultaneous search of effective source frequency and source azimuth displays a pattern of smoothly evolving sidelobes. The behavior of these sidelobes in the source frequency/azimuth plane can be determined by varying source frequency and source azimuth such that the received frequency remains unchanged. The result simplifies to

$$\frac{\delta\omega_s}{\omega_s} \approx \frac{v_r}{c_p}\sin[\theta_s - \psi_r]\delta\theta_s \quad (3)$$

For a single straight-line track traversed at constant speed, Eq. 3 describes the sinusoidally-varying slopes of the trajectory of the beamformer "grating lobe" in the frequency/azimuth plane. For a set of straight-line tracks, the true source frequency and azimuth are determined by the intersection of these trajectories.

2.2 Accounting for Vehicle Accelerations – the Resampling Beamformer

The quantity actually measured by the AUV-based digital data acquisition system is not the received frequency itself, but rather the fractional sampling frequency, given by the received frequency normalized by the data sampling rate, $\omega_r(t)/\Omega_0$. The variations in AUV velocity cause the received frequency to be dependent upon time so that the received energy from a single transmitted tone is spread across a finite band of frequencies over the time period of the long ffts required for low frequency Doppler beamforming. However, the sampling theorem[3] says that a continuous signal can be reconstructed exactly from equally-spaced digital samples of the signal as

long as the continuous signal is band-limited and that the digital sampling rate is more than twice the highest frequency component in the continuous signal. Therefore, the underlying continuous signals recorded by the AUV-mounted hydrophones can be reconstructed and redigitized at a time-varying sampling rate in order to exactly cancel known variations in AUV velocity. The requirement for canceling these AUV-motion-induced frequency variations is

$$\frac{d}{dt}\left(\frac{\omega_r(t)}{\Omega(t)}\right)=0 \;\rightarrow\; \frac{1}{\omega_r(t)}\frac{d\omega_r(t)}{dt}=\frac{1}{\Omega(t)}\frac{d\Omega(t)}{dt} \tag{4}$$

Integrating this equation and plugging in the expression for the received frequency from Eq. 2, the expression for the received fractional sampling frequency, η_r, after resampling based on an assumed source bearing of $\theta(\hat{l})$ given that the true source bearing is θ_s is

$$\eta_r(t)=\frac{\omega_r(t)}{\Omega(t)}=\left(\frac{\omega_s}{\Omega_0}(1+\frac{v_r^0}{c_p}\cos[\theta(\hat{l})-\psi_r^0])\right)\left(\frac{c_p+v_r(t)\cos[\theta_s-\psi_r(t)]}{c_p+v_r(t)\cos[\theta(\hat{l})-\psi_r(t)]}\right) \tag{5}$$

where the AUV speed, $v_r(t)$, and direction of motion, $\psi_r(t)$, are assumed to vary with time, $v_r^0 \equiv v_r(t_0)$, and similarly for ψ_r^0. The first term in brackets in Eq. 5 is independent of time and equals the assumed received fractional sampling frequency for the given look direction, $\hat{l}$. The second term in brackets contains the time dependence due to the variations in AUV velocity. When the assumed source bearing (look direction) equals the true source direction, then this second term becomes unity and η_r is time-independent. Simultaneously, the first term in brackets becomes equal to the "correct" received fractional sampling frequency. Therefore, the basis of the beamforming operation is the degradation in the output of the fft due to temporal variability in the fractional sampling frequency that arises from "mismatch" between the true and assumed source bearings. The number of frequency bins over which a single tone's energy is spread when the look direction does not correspond to the true source direction is determined by the fft length (i.e., the synthetic aperture array length). Eq. 5 also shows that the beamformer sensitivity (determined by the temporal variability of the fractional sampling frequency) increases with increasing source frequency and increasing temporal variations in AUV speed and heading (increasing acceleration).

Applying Eq. 5 to the special case of constant acceleration along a linear track ($dv_r/dt = \text{constant}$, $d\psi_r/dt = 0$), then η_r is independent of time both when $\theta(\hat{l}) = \theta_s$ and when $\theta(\hat{l}) = 2\psi_r(t) - \theta_s$. This ambiguity disappears when either $\psi_r(t) = \theta_s$ or $\psi_r(t) = \theta_s + \pi$, equivalent to the left-right ambiguity that exists when beamforming line arrays of omni-directional elements. In this case, the ambiguity occurs about the line formed by the direction of motion because the change in received frequency of a tone is the same whether the source is at a given angle clockwise from the direction of motion or at that same angle in the counterclockwise direction. In contrast, the case of circular motion at constant speed ($dv_r/dt = 0$, $d\psi_r/dt = \text{constant}$) displays an ambiguity at $\theta(\hat{l}) = \pi + 2\psi_r(t) - \theta_s$. That is, the left-right ambiguity occurs about a line perpendicular to the direction of motion and disappears at broadside ($\theta_s - \psi_r(t) = \pm\pi/2$). This ambiguity occurs because the increase in the Doppler-upshifted received frequency from a single tone source as the receiver's heading becomes more oriented towards the direction of source is the same as that due to a decrease in Doppler-downshifted frequency as the receiver's heading becomes less aligned with the direction heading away from the source. Since the vehicle heading is constantly changing along a circular arc, this ambiguity (sidelobe) decreases with increasing distance traveled along the arc.

This time-domain resampling approach is inherently broadband; it works for all frequencies simultaneously. Therefore, it is well suited for use with time-delay-and-sum beamforming, and can be used in conjunction with the Doppler beamforming methods discussed previously.

3 THE EXPERIMENT AND THE AUTONOMOUS VEHICLES

The data in this paper were collected during a 8-day experiment in April, 2004. The site was 67 km west of San Diego, CA at 32° 38.5' N, 117° 57.5' W (Fig. 1). R/P FLIP, a 100-m-long manned spar buoy, was deployed in 180-m water in a 3-point mooring. Acoustic sources, generating a variety of waveforms at depths from 10-50 m, were deployed from FLIP. The prop-driven AUV, whose tracks during one of its events are plotted in Fig. 1, was deployed and retrieved from R/V Sproul. Also shown in Fig. 1 are the locations of the 3 acoustic transponders that allowed the AUV location in 2D to be determined to sub-meter accuracy[4]. A total of 6 days of prop-driven AUV missions were conducted followed by two days of flights with the prototype flying wing underwater glider. Unfortunately, the glider flights were conducted at ranges too great for the FLIP-based source transmissions to be detected.

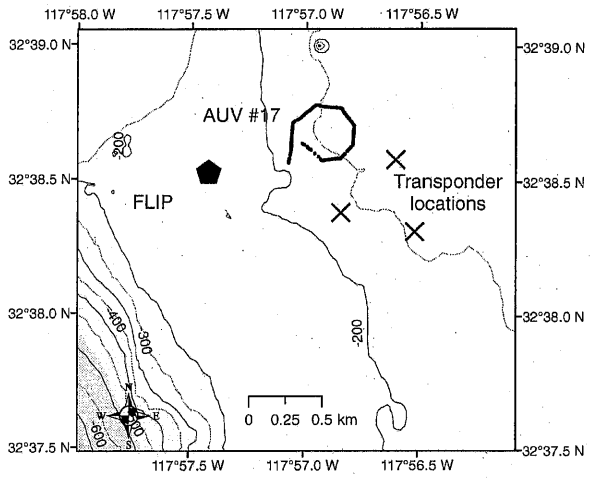

Figure 1. Map of the April, 2004 experiment site with bathymetry contours every 50 m.

The prop-driven AUV is an Odyssey IIb previously manufactured by Bluefin Robotics, Inc. (Fig. 2a). It is 2.2 m long, 0.58 m in diameter, and has a maximum speed and mission duration of 1.2 m/sec and 4 hours, respectively. The vehicle's standard propulsion system was replaced by the ducted-fan, vectored-thrust system presently installed on all modern Bluefin vehicles and then modified to reduce the radiated acoustic and vibration noise by 20-50 dB to typical ocean background noise levels above 300 Hz[1]. An 8-element hydrophone array with 10 kHz per channel bandwidth was mounted inside the outer shroud of the AUV to retain the vehicle's hydrodynamic properties. Total physical aperture of the array was about 1.3 m along the vehicle's length and 0.5 m in the cross vehicle direction.

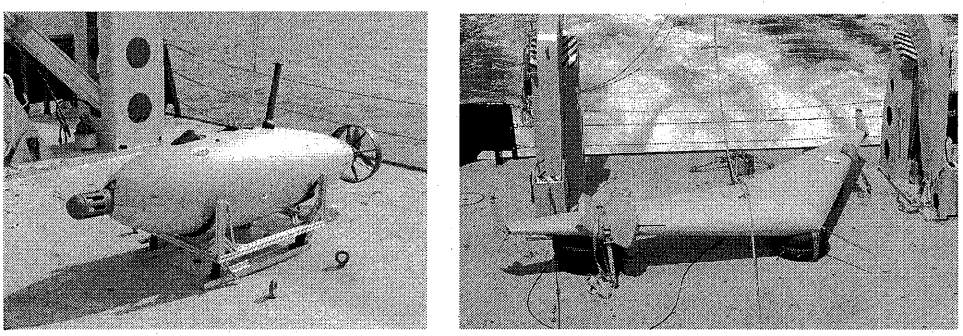

Figure 2. Photographs of the modified Odyssey IIb prop-driven AUV (left) and the prototype flying wing underwater glider (right), both shown on the fantail of R/V Sproul.

Stingray (Fig. 2b), a prototype buoyancy-driven glider of the flying wing design, has a 6.1 m wing span and 20 times the internal volume of other underwater gliders. It is designed to maximize horizontal transport efficiency by minimizing its glide slope. The tests in 2004 demonstrated an inverse glide slope (equal to the "lift-to-drag ratio") of 17/1, five times greater than other underwater gliders[5]. Up to four autonomously recording hydrophones with 4 kHz bandwidth were mounted in a symmetric 2D geometry inside the wing.

4 EXPERIMENTAL RESULTS

The received spectra from 6 of the 8 AUV-mounted hydrophones' data recorded along each of the 8 legs of the octagon event in Fig. 1 are plotted in Fig. 3a. (Leg 1 is the westernmost leg where the AUV was heading nearly due north and the direction of travel along the final leg 8 was to the northwest). For each leg number (listed along the vertical axis) the 6 horizontal lines in the plot represent the 6 single element spectra. In order to create an artificial source with exactly the same frequency content as the FLIP source but with 10 dB higher levels, the time series processed for leg 1 were generated by first multiplying those originally recorded along leg 1 by a factor of 0.3 (10 dB attenuation) and then adding those recorded during leg 3. Similarly, each subsequent leg's time series were attenuated by a factor of 0.3 and then added to those recorded two legs later in the sequence; e.g., leg 4's time series were added to the attenuated version of those from leg 2, those from leg 5 added to the attenuated leg 3 time series, etc. Given that the source on FLIP was located at an average bearing of 254° from the AUV tracks, this process created an artificial source with exactly the same frequency content but with 10 dB greater levels 90° counterclockwise from FLIP, at 164°. Each spectrum in Fig. 3a has a frequency resolution of 0.02 Hz and is plotted as a function of relative frequency, $(\omega_r - \omega_c)/\omega_c$, since the spectral estimates were obtained by averaging over four tones with center frequencies (ω_c) of 220, 280, 370, and 460 Hz.

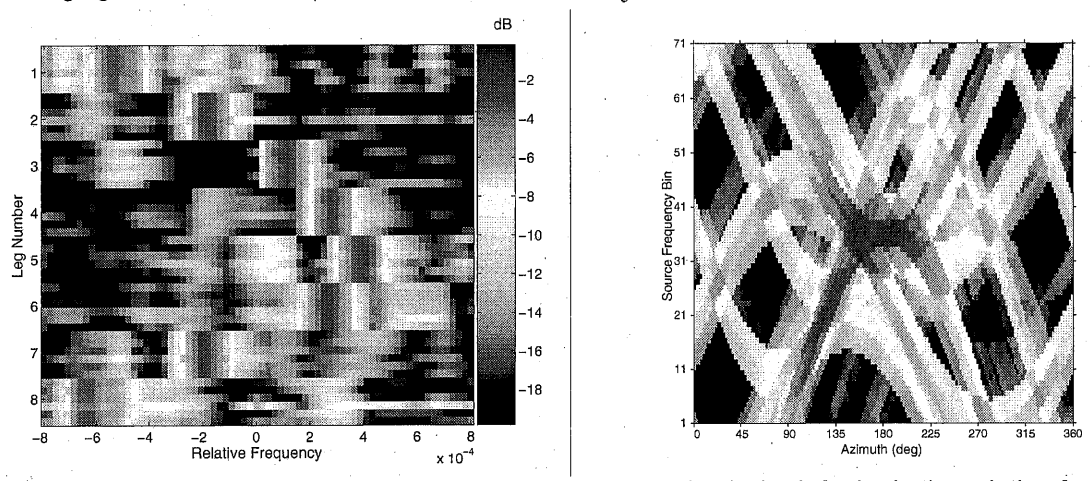

Figure 3. For each of the 8 legs of the octagon event in Fig. 1, the left plot is the relative frequency averaged over 4 tones, and the plot on the right is the simultaneous search over effective source frequency and source azimuth with data from a single hydrophone in a frequency band around the 220 Hz tone.

The results in Fig. 3a show that the lowest relative frequencies for the high-level source at 164° were measured along legs 1 and 8 since the AUV was traveling away from the source, whereas leg 5's spectra contain the highest relative frequencies since the motion was towards the source. The weaker source at 254° also can be detected in the figure, particularly along leg 3 at about -5 relative frequency and along leg 5 just above 0. Since this weaker source, by construction, generates exactly the same set of signals as the higher-level interferer, it would not be detectable by a fixed omni-directional receiver. By pushing and pulling energy around in the received spectrum, the motion of the AUV has improved detection under these anisotropic, spectrally non-white conditions.

These variations in received frequency as a function of AUV direction of motion can be combined in various ways to obtain directional estimates of the sound field. The results of simultaneously searching for source frequency and source azimuth using the Doppler beamforming method described in Sect. 2.1 applied to data collected by a single hydrophone in a frequency band around the 220 Hz source tone are plotted in Fig. 3b. A set of intersecting arcs are present in the figure; their behavior is described by Eq. (3). The intersection of the darkest red arcs (highest sidelobes) indicates the beamformer's best estimate of the azimuth and frequency of the high-level, 164°-azimuth source.

The results of applying Doppler/synthetic aperture beamforming with moving physical aperture for the octagon event in Fig. 1 are shown in the lower two curves in Fig. 4. For comparison, the upper two curves in the plot show the beamforming results using physical aperture only. The physical array was created by six hydrophones (the same six elements as in Fig. 3a) forming a 2D square-shaped array with approximate 0.5-m length per side. Both conventional and white-noise-constrained adaptive beamforming were applied to the physical aperture data. The figure shows that the overall dimension of the physical array, less than one-tenth of an acoustic wavelength at the source frequency of 220 Hz, is too small to resolve the presence of two sources even with adaptive beamforming. However, the combination of Doppler and physical aperture beamforming provides significantly improved results compared to either physical aperture alone or Doppler beamforming with a single omni-directional element (results not presented here show a narrower main lobe but significantly higher sidelobes). The combined adaptive/Doppler beamforming approach gives lower sidelobes than that using conventional/Doppler beamforming.

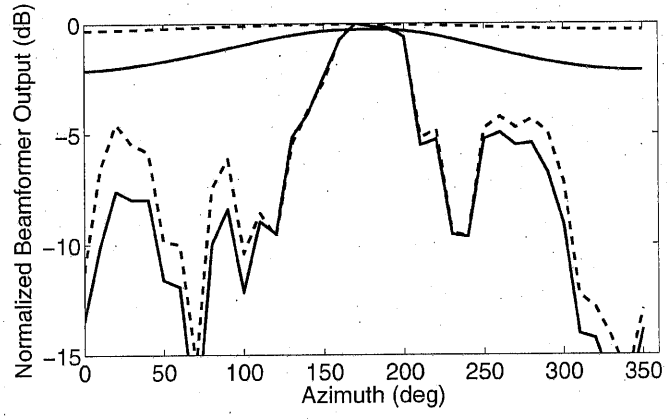

Figure 4. Beamformer output vs azimuth for the octagon event in Fig. 1. The lower two curves are the output of Doppler beamforming with moving physical aperture and the upper two curves use physical aperture only. Results from both conventional (dotted curves) and white-noise-constrained adaptive beamforming (solid curves) applied to the physical aperture data are shown.

The size of the octagon event with respect to the source/receiver range causes a broadening of the beamformer output peaks, and the main peak is further broadened due to the method of creating multi-source conditions. In the case of moving physical aperture, additional broadening of the high-level source peak occurs because the average heading of the AUV does not change by exactly the same amount from one leg to the next.

The properties of the resampling beamformer are dictated by the character of the vehicle acceleration. A special case with interesting properties is that of circular motion at constant speed. As motivation for examining this case, Fig. 5a shows the trajectory of Stingray as it ascended to the surface after being released from 155 m depth during its 6th flight in 2004. It executed nearly 10 complete circles with 30-40 m radii in the counterclockwise direction (as viewed downward from the ocean surface), demonstrating a station-keeping capability while traveling near its top horizontal speed (2.5 m/s). Numerical modeling shows that smaller turning radii at even higher speeds are achievable at steeper bank (roll) angles. As an extreme case, Fig. 5b shows the synthesized

resampling beamformer beam pattern for circular motion at constant speed (1.0 m/s) in the clockwise direction with a radius of curvature of 8.4 m. In the figure, the source is located at 0° azimuth and transmitting a 500 Hz tone. The resulting beam pattern shows a narrow main lobe with sidelobes at least 12 dB down from the main lobe peak level. This performance is achieved due to the spectral smearing effects of the centripetal acceleration associated with the small radius of curvature.

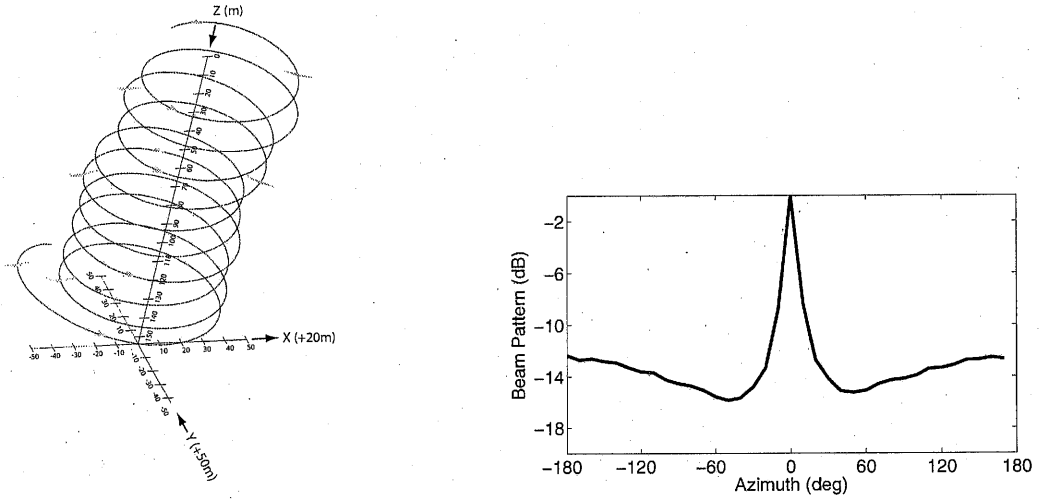

Figure 5. Stingray's trajectory in 3D as it ascended to the surface from 155 m depth during flight 6 in April, 2004 (left) and the synthesized resampling beamformer plane wave response for a 500 Hz tone source at 0° azimuth while traversing an 8.4-m radius circle at a fixed speed of 1.0 m/s (right).

Significant vehicle accelerations at a fairly constant speed occurred during the sequence of 45° turns from one straight track to the next in the AUV event shown in Fig. 1. During the first turn, from a heading of due north to 45° east of north, the acoustic source deployed from FLIP was approximately endfire to the arc of the turn. The AUV navigation data recorded during the turn indicate that the vehicle's direction of motion actually rotated through an angle of 60° and its speed increased from 0.9 m/s to 1.0 m/s while stabilizing on the northeast track. The results of resampling 6 of the 8 individual AUV hydrophone time series for the 370 Hz tone transmitted from FLIP are displayed in Fig. 6. The original hydrophone time series recorded at sea were used in the processing rather than the artificial multi-source data set used in the previous part of this section. In addition to the main lobe, a high side lobe exists in the 10-50° azimuth interval. It is due to the ambiguity about the broadside direction for circular-type motion (Sect. 2.2). That is, given the average AUV direction of motion during the turn was about 35° so that broadside was at 125°, then the main beam at -130° (true source azimuth of 230°) should have a corresponding high sidelobe around 20°.

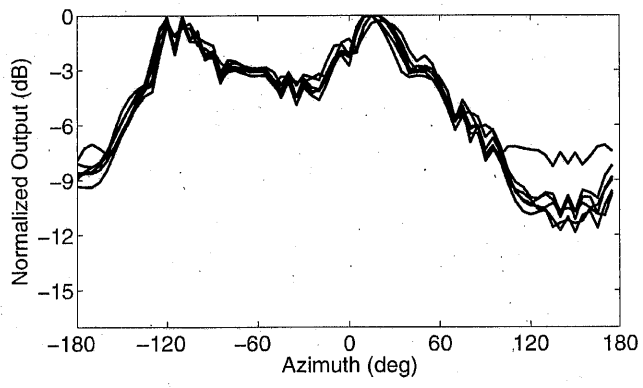

Figure 6. Resampling beamformer output for the 370 Hz source tone using data from each of 6 hydrophones during the first 45° turn of the octagon event in Fig. 1.

5 CONCLUSIONS

Underwater autonomous vehicles with hull-mounted passive sonar arrays provide unique opportunities for measuring ocean acoustic fields. They have the ability to adapt and maneuver in response to received sounds in their environment. Even more so, they can alter the structure of received signals to optimize extraction of information of interest. One way of actively modifying the character of received sounds is through motion, as illustrated in this paper. However, motion requires expenditure of energy, in limited supply on autonomous vehicles. Therefore, these energy costs must be accounted for in developing vehicle measurement strategies. In fact, the characteristics of the autonomous vehicle,
e.g., its maneuverability and energy efficiency, become an integral part of the signal and array processing.

6 ACKNOWLEDGMENTS

Dennis Rimington and David Price helped provide engineering support for the prop-driven AUV operations and Aaron Thode led the at-sea flying wing glider deployments. Galina Rovner did most of the data processing. Dave Ensberg, Heidi Batchelor, Dave Chadwell, and Neil Kussat also helped with at-sea data collection. All these individuals work at the Marine Physical Laboratory, Scripps Institution of Oceanography. Finally, the assistance of the crews of the R/P FLIP and R/V Sproul is greatly appreciated.

Much of the results presented here will appear in "Active control of passive acoustic fields: Passive synthetic aperture/Doppler beamforming with data from an autonomous vehicle" in the Journal of the Acoustical Society of America. The flight characteristics of Stingray will be published in the IEEE Journal of Oceanic Engineering[5].

This work was supported by the Office of Naval Research, Code 321(US) as part of MPL's Applied Research Laboratory program and Code 321(OE) in the flying wing glider development.

7 REFERENCES

1. R. Zimmerman, G.L. D'Spain, and C.D. Chadwell, `Decreasing the radiated acoustic and vibration noise of a mid-size AUV', IEEE J. Oceanic Engin. 30(1) 179-187 (2005).
2. A.D. Pierce. Acoustics; An Introduction to Its Physical Principles and Applications, Acoustical Society of America, New York (1989).
3. J.S. Bendat and A.G. Piersol. Random Data: Analysis and Measurement Procedures, 2nd ed John Wiley and Sons, New York (1986).
4. N.H. Kussat, C.D. Chadwell, and R. Zimmerman, `Absolute positioning of an autonomous underwater vehicle using GPS and acoustic measurements', IEEE J. Oceanic Engin. 30(1), 153-164 (2005).
5. S.A. Jenkins, G.L. D'Spain, G. Rovner, and A.M. Thode. `Hydrodynamics and acoustics of a flying wing underwater glider in free flight', accepted for publ. IEEE J. Oceanic Engin., 50 pgs plus 15 figs.